CONFERÊNCIA NACIONAL DE MÉTODOS NUMÉRICOS EM
MECÂNICA DOS FLUIDOS E TERMODINÂMICA 2006
FCT-UNL, Monte de Caparica, 8 e 9 de Junho, 2006

DEVELOPMENT OF A REYNOLDS STRESS MODEL TO PREDICT TURBULENT FLOWS WITH VISCOELASTIC FLUIDS

P. R. Resende[1], F. T. Pinho[1,2], D. O. Cruz [3]

1: Centro de Estudos de Fenómenos de Transporte
Faculdade de Engenharia da Universidade do Porto
Rua Dr. Roberto Frias s/n,
4200 – 465 Porto, Portugal
e-mail: resende@fe.up.pt

2: Universidade do Minho
Largo do Paço
4704-553 Braga, Portugal
e-mail: fpinho@fe.up.pt

3: DEM – Universidade Federal do Pará
Campus Universitário do Guamá
66075 – 900 Belém, Pará, Brazil
e-mail: doac@ufpa.br

Keywords: Turbulence model, drag reduction, polymer solutions, second order closure.

Abstract: *A second order closure for predicting turbulent flows of viscoelastic fluids is proposed in this work and its performance is assessed by comparing its predictions with experimental data for fully-developed pipe flow. The model is an extension of an existing Reynolds stress closure for Newtonian fluids and includes low Reynolds number damping functions to properly deal with wall effects. The model was modified to take into account viscoelasticity, especially in the pressure strain term. The new damping functions depend on rheological characteristics of the fluids, as was the case with previous developments of k-ε models for viscoelastic fluids by Cruz and Pinho [1] and Cruz et al. [2].*

1. INTRODUCTION

A Reynolds stress model is developed to predict turbulent flows with viscoelastic fluids and is tested here in fully-developed channel flows of polymer solutions. First-order turbulence models have shortcomings when it comes to predicting flows with separation or streamline curvature, amongst other things (see an early revision in Patel et al. [3]). In addition, viscoelastic fluids in duct flows exhibit stronger anisotropy of the Reynolds stress tensor than Newtonian fluids do, which further accentuates the shortcomings of some first-order closures to properly deal with them. The use of anisotropic first-order models can offset some of these disadvantages (Park et al. [4], Craft et al. [5]). Now that simple first-order turbulence closures are available for viscoelastic fluids (Resende et al. [6]), and have been tested in duct flow, it is

time to evolve to higher-order closures which will enable the handling of more complex flows, such as flows with separation.

The first turbulence models for viscoelastic fluids date from the 1970's with Mizushina et al. [7], Durst and Rastogi [8] and Poreh and Hassid [9]. Their scope was rather limited because they depended on parameters that needed to be selected for each fluid in each flow situation. In the 1980's new turbulence models appeared (Politis [10], Malin [11]), but were limited to the inelastic fluids of variable viscosity. To overcome this limitation Pinho [12] and Cruz and Pinho [1] developed a turbulence model using a modified version of the generalized Newtonian constitutive equation in order to account elastic effects and therefore introduce rheological parameters into the turbulence model. Subsequent developments of that model were introduced by Cruz et al. [2] and Resende et al. [6].

The present Reynolds stress closure is a step forward in the hierarchy of models for viscoelastic fluids and is based on the model of Lai and So [13] for Newtonian fluids. This model was selected because it combined simplicity with a low Reynolds number capability, essential for use with viscoelastic fluids for which no universal law of the wall exists. The performance of the model is tested against experimental data for dilute polymeric aqueous solutions of Escudier et al. [14] and Resende et al [6] and also against results from the DNS simulation for a FENE-P model of Dimitropoulos et al. [15].

The next section presents the governing equations for viscoelastic turbulent flow. The terms requiring modeling are identified in the Section 3 with the corresponding closures. The results of the numerical simulations and their discussion are presented in Section 4. The paper closes with a summary of the main conclusions.

2. GOVERNING EQUATIONS

The governing equations are the continuity and momentum equations and the Reynolds stress is calculated by its transport equation. The extra stress of the fluid is given by a generalized Newtonian constitutive equation modified by Pinho [12]. The momentum equation is

$$\rho\frac{\partial U_i}{\partial t}+\rho U_k\frac{\partial U_i}{\partial x_k}=-\frac{\partial \overline{p}}{\partial x_i}+\frac{\partial}{\partial x_k}\left(2\overline{\mu}S_{ik}-\rho\overline{u_iu_k}+2\overline{\mu' s_{ik}}\right) \tag{1}$$

where p is the pressure, $\overline{\mu}$ is the average molecular viscosity, u_i is the i-velocity component and S_{ij} is the rate of deformation tensor defined as $S_{ij}\equiv\left(u_{i,j}+u_{j,i}\right)/2$. Here, and elsewhere, small letters or a prime indicate fluctuations, capital letters or an overbar designate time-average quantities and a hat is used for instantaneous values.

The average molecular viscosity ($\overline{\mu}$) is given by equation (2) which combines the pure viscometric shear viscosity contribution (η_V) in eq. (3), with the high Reynolds number time-average molecular viscosity contribution ($\overline{\mu}_h$) of eq. (4).

$$\overline{\mu}=f_v\overline{\mu}_h+(1-f_v)\eta_v, \tag{2}$$

$$\eta_v=K_v\left[\dot{\gamma}^2\right]^{(n-1)/2}, \tag{3}$$

$$\overline{\mu}_h = \left(C_\mu \rho\right)^{3m(m-1)A_2/(8+3m(m-1)A_2)} \times 2^{4m(m-1)A_2/(8+3m(m-1)A_2)} \times k^{6m(m-1)A_2/(8+3m(m-1)A_2)} \times \varepsilon^{([8-3(M-1)A_2]m)/(8+3m(m-1)A_2)} \times B^{8/(8+3m(m-1)A_2)} \tag{4}$$

where K_v and n are the power law parameters, f_v is a damping function equal to f_μ and k and ε represent the turbulent kinetic energy and its rate of dissipation, respectively. This model for $\overline{\mu}$ was derived by Pinho [12].

The pseudo- elastic stress in the momentum equation ($2\overline{\mu' s_{ik}}$) and the new terms of the transport equation for Reynolds stress ($\rho\overline{u_i u_k}$) require specific modelling which is presented in the next section.

The transport equation for Reynolds stress is

$$\begin{aligned}
&\rho\frac{D\overline{u_i u_j}}{Dt} + \rho\overline{u_j u_k}\frac{\partial U_i}{\partial x_k} + \rho\overline{u_i u_k}\frac{\partial U_j}{\partial x_k} = -\rho\frac{\partial}{\partial x_k}\overline{u_i u_j u_k} - \left(\frac{\partial}{\partial x_i}\overline{p' u_j} + \frac{\partial}{\partial x_j}\overline{p' u_i}\right) + \\
&+\overline{p'\left(\frac{\partial u_j}{\partial x_i} + \frac{\partial u_i}{\partial x_j}\right)} + \overline{\mu}\frac{\partial^2 \overline{u_i u_j}}{\partial x_k \partial x_k} - 2\overline{\mu}\overline{\frac{\partial u_i}{\partial x_k}\frac{\partial u_j}{\partial x_k}} + \frac{\partial \overline{\mu}}{\partial x_k}\frac{\partial \overline{u_i u_j}}{\partial x_k} \\
&+\frac{\partial \overline{\mu}}{\partial x_k}\left(\frac{\partial \overline{u_k u_j}}{\partial x_i} + \frac{\partial \overline{u_k u_i}}{\partial x_j} - 2\overline{u_k s_{ij}}\right) + \overline{\mu'\frac{\partial^2 u_i u_j}{\partial x_k \partial x_k}} - 2\overline{\mu'\frac{\partial u_i}{\partial x_k}\frac{\partial u_j}{\partial x_k}} \\
&+\overline{\frac{\partial \mu'}{\partial x_k}\frac{\partial u_i u_j}{\partial x_k}} + \overline{\frac{\partial \mu'}{\partial x_k}\left(u_j\frac{\partial u_k}{\partial x_i} + u_i\frac{\partial u_k}{\partial x_j}\right)} + \overline{\mu' u_j}\frac{\partial^2 U_i}{\partial x_k \partial x_k} \\
&+\overline{\mu' u_i}\frac{\partial^2 U_j}{\partial x_k \partial x_k} + \overline{u_j\frac{\partial \mu'}{\partial x_k}\left(\frac{\partial U_i}{\partial x_k} + \frac{\partial U_k}{\partial x_i}\right)} + \overline{u_i\frac{\partial \mu'}{\partial x_k}\left(\frac{\partial U_j}{\partial x_k} + \frac{\partial U_k}{\partial x_j}\right)}
\end{aligned} \tag{5}$$

3. CLOSURES FOR NON-NEWTONIAN TERMS

We start with the two molecular related stresses in the momentum equation. Term $2\overline{\mu' s_{ik}}$ was designated a pseudo-elastic stress by Cruz et al. [2] where a closure was proposed in the context of their k-ε model. Inspired by their derivation, we propose here an extended version consistent with the use of a full Reynolds stress model. Therefore, the expression for the pseudo-elastic stress used here is

$$2\overline{\mu' s_{ij}} = \tilde{C}\frac{K_v K_e}{A_\varepsilon^{\,p-1}}\left[\frac{\rho\left|\overline{u_i u_j}\right|}{2\overline{\mu}}\frac{\partial U_i}{\partial x_j}\right]^{\frac{(p+n-2)}{2}} \times \frac{1}{L_c} \times \frac{\overline{u_i u_j}}{\sqrt{\left|\overline{u_i u_j}\right|}} \tag{6}$$

with

$$\tilde{C} = \left(1 + C_0\right)^{p+n-2} - 1 \tag{7}$$

The pseudo-elastic stress vanishes in the Newtonian limit (n=1 and p=1), an effect properly accounted for by parameter $\tilde{C}$, which depends on parameter C_0. This parameter takes on a

new value different from that in Cruz et al. [2] and was obtained from optimization of the Reynolds stress model predictions.
In the Reynolds stress transport equation we identify terms which are identical in form to those for Newtonian fluids and new terms associated with the non-Newtonian fluid characteristics, which are those involving fluctuating viscosities. Of these, according to the order of magnitude analysis made by Pinho [12], the following terms could be neglected:

$$\overline{u_j \frac{\partial \mu'}{\partial x_k}\left(\frac{\partial U_i}{\partial x_k}+\frac{\partial U_k}{\partial x_i}\right)}+\overline{u_i \frac{\partial \mu'}{\partial x_k}\left(\frac{\partial U_j}{\partial x_k}+\frac{\partial U_k}{\partial x_j}\right)} \tag{8}$$

$$\overline{\mu' u_j}\frac{\partial^2 U_i}{\partial x_k \partial x_k}+\overline{\mu' u_i}\frac{\partial^2 U_j}{\partial x_k \partial x_k} \tag{9}$$

The remaining non-Newtonian terms are modelled as follows assuming high Reynolds number turbulence:

$$\frac{\partial \overline{\mu}}{\partial x_k}\frac{\partial \overline{u_i u_j}}{\partial x_k}+\overline{\frac{\partial \mu'}{\partial x_k}\frac{\partial u_i u_j}{\partial x_k}} \sim C_{V1}\times \frac{\partial \overline{\mu}}{\partial x_k}\frac{\partial \overline{u_i u_j}}{\partial x_k} \tag{10}$$

$$\frac{\partial \overline{\mu}}{\partial x_k}\left(\frac{\partial \overline{u_k u_j}}{\partial x_i}+\frac{\partial \overline{u_k u_i}}{\partial x_j}-2\overline{u_k s_{ij}}\right)+\overline{\frac{\partial \mu'}{\partial x_k}\left(u_j\frac{\partial u_k}{\partial x_i}+u_i\frac{\partial u_k}{\partial x_j}\right)} \sim C_{V2}\times \frac{\partial \overline{\mu}}{\partial x_k}\left(\frac{\partial \overline{u_k u_j}}{\partial x_i}+\frac{\partial \overline{u_k u_i}}{\partial x_j}\right) \tag{11}$$

where C_{V1} and C_{V2} are parameters to be quantified later.
All the other terms are Newtonian and are modelled according to the original model of Lai and So [13]:

- Turbulent diffusion of the Reynolds stresses, D_{ij}^T,

$$-\rho\frac{\partial}{\partial x_k}\overline{u_i u_j u_k}=\rho\frac{\partial}{\partial x_k}\left\{C_s\frac{k}{\varepsilon}\left[\overline{u_i u_l}\frac{\partial \overline{u_j u_k}}{\partial x_l}+\overline{u_j u_l}\frac{\partial \overline{u_k u_i}}{\partial x_l}+\overline{u_k u_l}\frac{\partial \overline{u_i u_j}}{\partial x_l}\right]\right\} \tag{12}$$

- The molecular diffusion of the Reynolds stresses, D_{ij}^v,

$$\overline{\mu}\frac{\partial^2 \overline{u_i u_j}}{\partial x_k \partial x_k}+\overline{\mu'\frac{\partial^2 u_i u_j}{\partial x_k \partial x_k}} \approx \overline{\mu}\frac{\partial^2 \overline{u_i u_j}}{\partial x_k \partial x_k}, \tag{13}$$

assuming at this stage a lack of correlation between fluctuating viscosity and the fluctuating second derivative of the Reynolds stress.

- The dissipation of the Reynolds stresses, ε_{ij},

$$-2\overline{\mu}\overline{\frac{\partial u_i}{\partial x_k}\frac{\partial u_j}{\partial x_k}}-2\overline{\mu'\frac{\partial u_i}{\partial x_k}\frac{\partial u_j}{\partial x_k}}=\rho\varepsilon_{ij}, \tag{14}$$

is modelled considering anisotropy and directional effects near walls, by

$$\varepsilon_{ij} = \frac{2}{3}\varepsilon\left(1-f_{w,1}\right)\delta_{ij} + \frac{f_{w,1}\left(\varepsilon/k\right)\left[\overline{u_i u_j} + \overline{u_i u_k}n_k n_j + \overline{u_j u_k}n_k n_i + n_i n_j \overline{u_k u_l}n_k n_l\right]}{1+3\overline{u_k u_l}n_l n_k/2k}, \tag{15}$$

- The pressure-strain, ϕ_{ij}^*,

$$-\left(\frac{\partial}{\partial x_i}\overline{p'u_j} + \frac{\partial}{\partial x_j}\overline{p'u_i}\right) + \overline{p'\left(\frac{\partial u_j}{\partial x_i} + \frac{\partial u_i}{\partial x_j}\right)} = \phi_{ij}^*, \tag{16}$$

is modelled by equation (17) considering the high Reynolds number contribution, ϕ_{ij}, and the wall approximation contribution, $\phi_{ij,w}f_{w,1}$.

$$\phi_{ij}^* = \phi_{ij} + \phi_{ij,w}f_{w,1}, \tag{17}$$

with

$$\phi_{ij,1} = -C_1\frac{\varepsilon}{k}\left(\overline{u_i u_j} - \frac{2}{3}k\delta_{ij}\right) - \alpha\left(P_{ij} - \frac{2}{3}\tilde{P}\delta_{ij}\right) - \beta\left(D_{ij} - \frac{2}{3}\tilde{P}\delta_{ij}\right) - \gamma k\left(\frac{\partial U_i}{\partial x_j} + \frac{\partial U_j}{\partial x_i}\right), \tag{18}$$

$$\phi_{ij,w} = C_1\frac{\varepsilon}{k}\left(\overline{u_i u_j} - \frac{2}{3}k\delta_{ij}\right) - \frac{\varepsilon}{k}\left(\overline{u_i u_k}n_k n_j + \overline{u_j u_k}n_k n_i\right) - \alpha^*\left(P_{ij} - \frac{2}{3}\tilde{P}\delta_{ij}\right), \tag{19}$$

where

$$D_{ij} = \left[\overline{u_i u_k}\frac{\partial U_k}{\partial x_j} + \overline{u_j u_k}\frac{\partial U_k}{\partial x_i}\right], \tilde{P} = \frac{1}{2}P_{ii}, \alpha = \frac{\left(8+C_2\right)}{11}, \beta = \frac{\left(8C_2-2\right)}{11}, \gamma = \frac{\left(30C_2-2\right)}{55}, \tag{20}$$

The transport equation for the rate of dissipation of turbulent kinetic energy of Lai and So's model [13] is used without any modification and is given by

$$\begin{aligned}\frac{D\varepsilon}{Dt} = {} & \frac{\partial}{\partial x_k}\left(\nu\frac{\partial\varepsilon}{\partial x_k}\right) + \frac{\partial}{\partial x_k}\left(C_s\frac{k}{\varepsilon}\overline{u_k u_i}\frac{\partial\varepsilon}{\partial x_i}\right) + C_{\varepsilon_1}\left(1+\sigma f_{w,2}\right)\frac{\varepsilon}{k}\tilde{P} - \\ & -C_{\varepsilon_2}f_\varepsilon\frac{\varepsilon\tilde{\varepsilon}}{k} + f_{w,2}\left[\left(\frac{7}{9}C_{\varepsilon_2} - 2\right)\frac{\varepsilon\tilde{\varepsilon}}{k} - \frac{1}{2k}\left(\varepsilon - \frac{2\nu k}{y^2}\right)^2\right]\end{aligned}, \tag{21}$$

with

$$\tilde{\varepsilon} = \varepsilon - 2\nu\left(\frac{\partial k^{1/2}}{\partial x_y}\right)^2, \tag{22}$$

Finally, the various parameters constants and damping functions are given in the next table.

Constants				
$C_1 = 1.5$	$C_2 = 0.4$	$C_{\varepsilon_1} = 1.35$	$C_{\varepsilon_2} = 1.8$	$C_s = 0.11$
$\alpha^* = 0.45$	$C_\varepsilon = 0.15$	$C_{V1} = -1.7$	$C_{V2} = 0.2$	$C_0 = -0.95$

Damping functions	
$f_{w,2} = \exp\left[-\left(\frac{R_T}{64}\right)^2\right]$	$f_\varepsilon = 1-\left(\frac{2}{9}\right)\exp\left[-\left(\frac{R_T}{6}\right)^2\right]$

Table 1 – Constants and damping functions of the Lai and So [13] Reynolds stress model

The turbulent Reynolds number, R_T, is defined as

$$R_T = \nu k^2 / \varepsilon, \tag{23}$$

The damping function $f_{w,1}$ of Lai an So [13] was modified to account for viscoelastic effects and is given by

$$f_{w,1} = \exp\left[-\left(\frac{f_\mu}{0.4}\right)^{1.1}\right], \tag{24}$$

where f_μ is the original damping function derived by Cruz and Pinho [1] in the context of their k-ε model.

$$f_\mu = \left\{1-\left[1+\left|\frac{1-n}{1+n}\right| y^+\right]^{-\left|1+n/1-n\right|/A^+}\right\} \times \left\{1-\left[1+\left|\frac{p-1}{3-p}\right| y^+ C^{\frac{1-p}{2-p}}\right]^{-\left|3-p/p-1\right|/A^+}\right\}, \tag{25}$$

This function accounts for wall effects very much as Van Driest's function do for Newtonian fluids and is influenced by the rheological properties of the fluids measured by the shear-thinning intensity (n<1) and Trouton ratio thickening (p>1) of the extensional viscosity. The parameters, which were quantified by performing extensive calculations, are identical to C=25 and A^+=35, and y^+ is the wall coordinate normalised by the wall viscosity $\left(y^+ = u_\tau y/\nu_w\right)$.

4. RESULTS AND DISCUSSION

The program used to carry out the numerical simulations is based on a finite-volume discretization and the TDMA solver is used to calculate the solution of the discretized algebraic governing equations. The mesh is non-uniform with 199 cells across the pipe, giving mesh-independent results for Newtonian and non-Newtonian fluids within 0.1%. The full domain in the transverse direction is mapped, hence only the following wall boundary conditions need to be imposed:

$$U = \overline{uu} = \overline{vv} = \overline{ww} = \overline{uv} = 0 \quad \text{and} \quad \varepsilon = 2\nu\left(\frac{\partial k^{1/2}}{\partial y}\right)^2 \quad \text{at} \quad r = R$$

The turbulence model was calibrated using the experimental data from Escudier et al. [14] for their 0.125% PAA aqueous solution, following the philosophy of Cruz and Pinho [1], Cruz et al. [2] and Resende et al. [6]. Then, the model is tested for the remaining viscoelastic fluids,

0.2% XG, 0.25% CMC and 0.09% / 0.09% XG / CMC without any change to the turbulence model. Finally a comparison is made also with the DNS results of Dimitropoulos et al. [15] for a FENE-P model with L=10.

4.1. Newtonian fluids

The modification of the damping function $f_{w,1}$ can severely affect predictions for Newtonian fluids, so here we assess that effect. The modification of $f_{w,1}$ was carried out to bring into the model the capability to predict flows of viscoelastic fluids, but the changes relative to the predictions with the original formulation of Lai and So [13] were minimized. For Newtonian fluids the error in the Darcy friction coefficient for fully-developed pipe turbulent flows, for a Reynolds numbers of 7430, is 8% relative to Blasius equation, and of 10% relative to the predictions with the original model of Lai and So [13]. This can also be observed in the comparison between the mean velocity profiles in wall coordinates in Fig. 1. At larger Reynolds numbers, however, the differences relative to the predictions of the original Lai and So model are negligible.

The corresponding profiles of the normalized turbulent kinetic energy and Reynolds normal stresses can be observed in the Fig. 2. Comparing the results of the present model with those model of Lai and So [13] we can see improvements in terms of the maximum value of the turbulent kinetic energy predictions and consequently a better distribution of the normalised Reynolds normal stresses, defined in Eq. (26),

$$u'^{+} = \sqrt{\overline{u^2}}\Big/u_\tau \; ; v'^{+} = \sqrt{\overline{v^2}}\Big/u_\tau \; ; w'^{+} = \sqrt{\overline{w^2}}\Big/u_\tau \; , \tag{26}$$

where u_τ is the friction velocity.

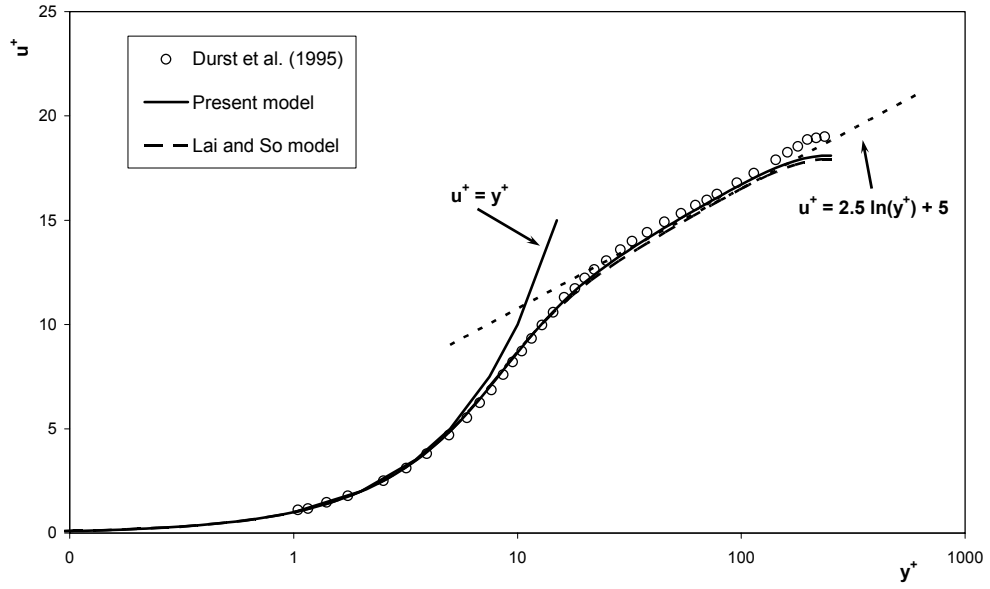

Fig. 1 – Comparison between the predicted and the measured mean velocity profile for fully-developed turbulent pipe flow of Newtonian fluid at Re=7430 in wall coordinates.

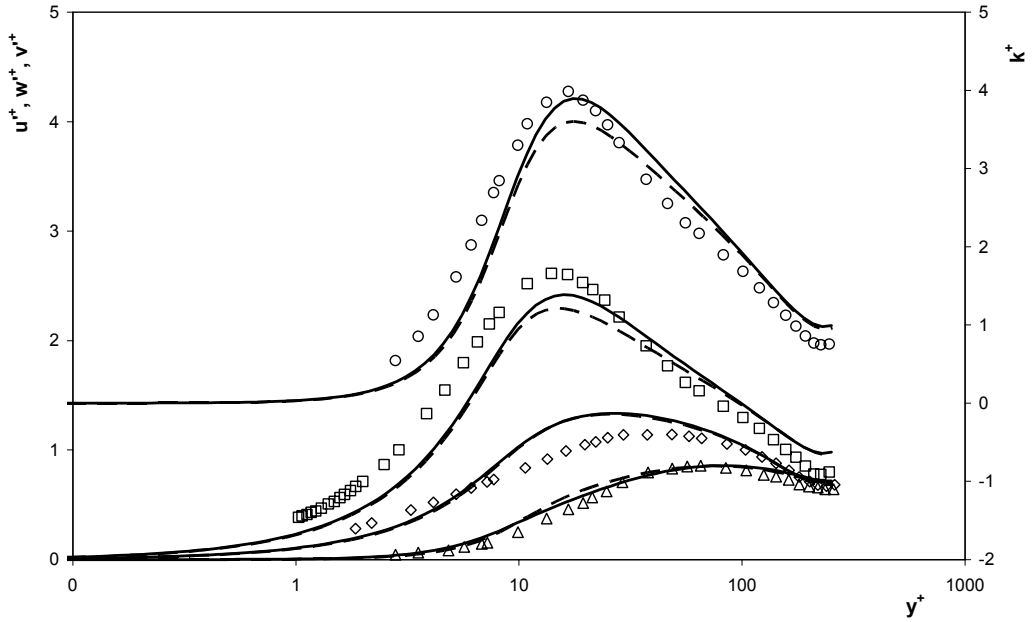

Fig. 2 – Comparison between the predicted and the measured profiles of normalized turbulent kinetic energy and Reynolds normal stresses for fully-developed turbulent pipe flow of Newtonian fluid at Re=7430 in wall coordinates: ○ k^+, □ u'^+, ◊ w'^+, Δ v'^+ data of Durst et al. [16]; — Present model; - - Lai and So model [13].

4.2. Non-Newtonian fluids

First we compare predictions with the experimental data for turbulent fully-developed pipe flow of Escudier et al. [14] and Resende et al. [6] followed by predictions with DNS data for channel turbulent flows of Dimitropoulos et al. [15].

The various non-Newtonian terms in the momentum and Reynolds stress equation have an impact at different locations in the flow. The pseudo-elastic stress in the momentum equation is basically relevant in the buffer layer, but this is sufficient to affect the flow across the whole pipe and is especially important to create drag reduction. Indeed, and in contrast to the $k-\varepsilon$ model of Cruz et al. [2], where the drag reduction was basically achieved by a reduction of the eddy viscosity, this Reynolds stress model is truer to the real behaviour of polymer solutions because the drag reduction is achieved by the increasing importance of this new stress as it should according to DNS simulations that show the drag reduction being achieved by the increasing role of the polymer stress (τ_p). In this Reynolds stress model, the pseudo-elastic stress values are larger than in the model of Cruz et al [2], but they still have a negative sign. This negative sign is not a deficiency of the model because the polymer contribution to the total extra stress equals the sum of the pseudo-elastic stress with part of the molecular shear stress, i.e. $\tau_p = 2\bar{\mu}S_{xy} + 2\overline{\mu' s_{xy}} - 2\mu_s S_{xy}$ where μ_s is the solvent viscosity (in the present case water). Therefore, the polymer shear stress remains positive, increases with drag reduction, as it should, and when added to the positive Reynolds shear stress and positive solvent shear stress the total equals the linear stress variation across the pipe. This is so even

though the deduction of the model for the pseudo-elastic stress was based in the same philosophy of Cruz et al. [2].
As the pseudo-elastic stress increases with drag reduction there is also a small increase of k^+, an improvement over the $k-\varepsilon$ closure developed by Cruz et al. [2]. Finally, and in contrast to the $k-\varepsilon$ model where the pseudo-elastic stress helped to improve the predictions, but was not essential to obtain drag reduction, in the Reynolds stress closure its incorporation in the balance of momentum is essential to obtain drag reduction, and the new non-Newtonian terms in the transport equation are also required.

4.2.1. Measured polymer solutions

The variation of the Darcy friction factor with Reynolds number for the 0.125% PAA solution can be observed in Fig. 3, and the corresponding mean velocity profile in wall coordinates for *Re*=42900 in Fig. 4. The predictions of both quantities compare well with the experimental data, except at low Reynolds number where there is a small difference of about 16 % at *Re*=10000. The variation of *f* versus *Re* is similar to that seen with the previous model of Cruz et al. [2].
The profiles of turbulent kinetic energy and of the Reynolds normal stresses in Fig. 5 show that *k* and $\overline{u^2}$ are underpredicted near to the wall, especially in the region of the peak stress. The prediction of $\overline{w^2}$ is good, but there is also an underprediction of $\overline{v^2}$.

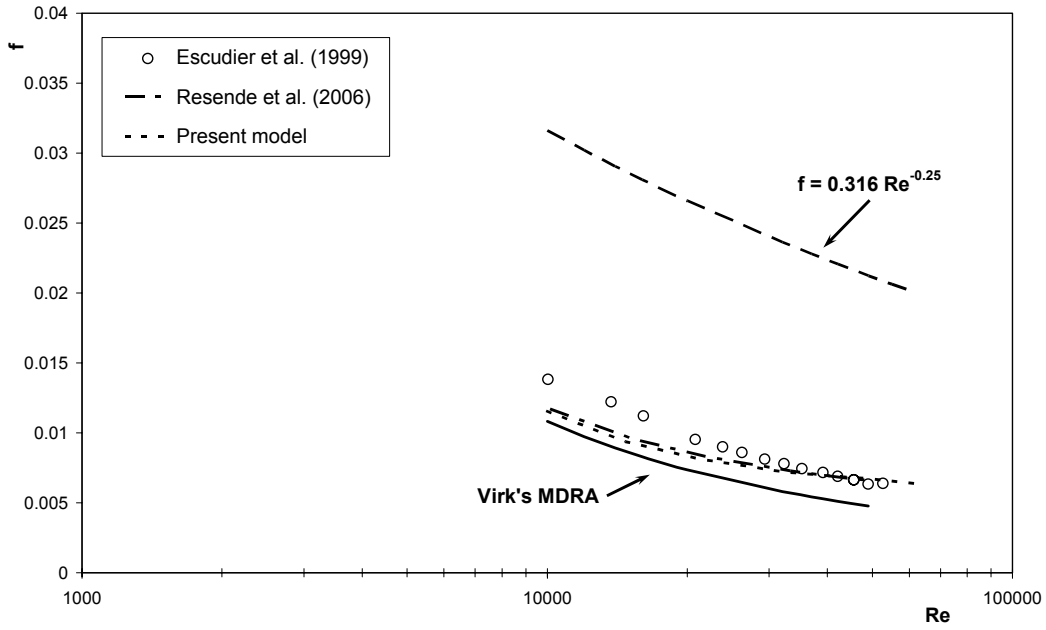

Fig. 3 – Comparison between predictions and measurements of Darcy friction factor in wall coordinates for fully-developed pipe turbulent flow with 0.125% PAA fluid.

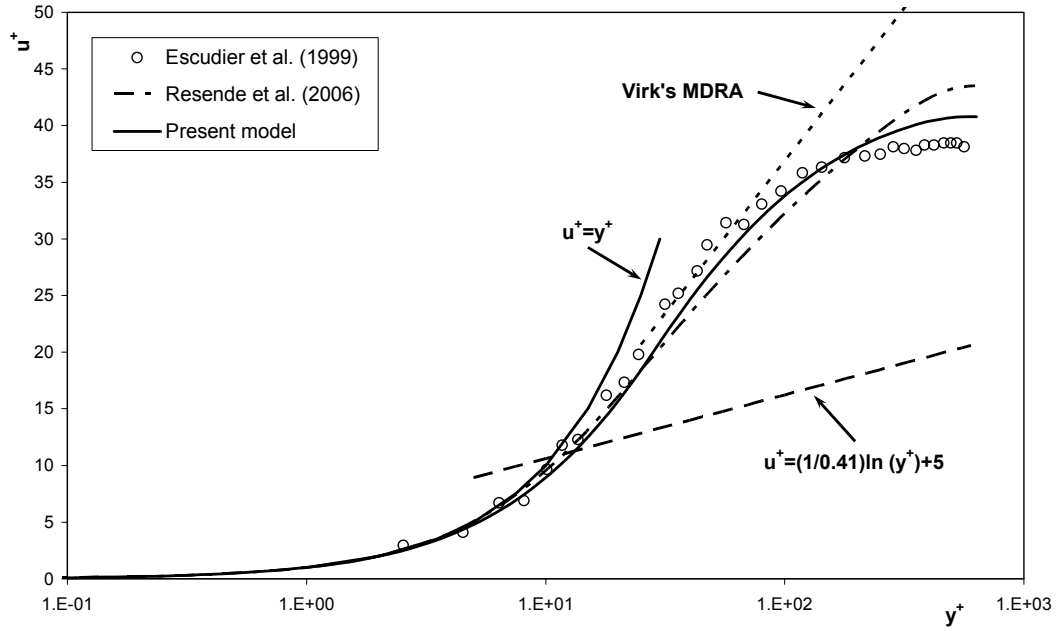

Fig. 4 – Comparison between the predicted and measured mean velocity profile for fully-developed pipe turbulent flow with the 0.125% PAA solution at Re=42900 in wall coordinates.

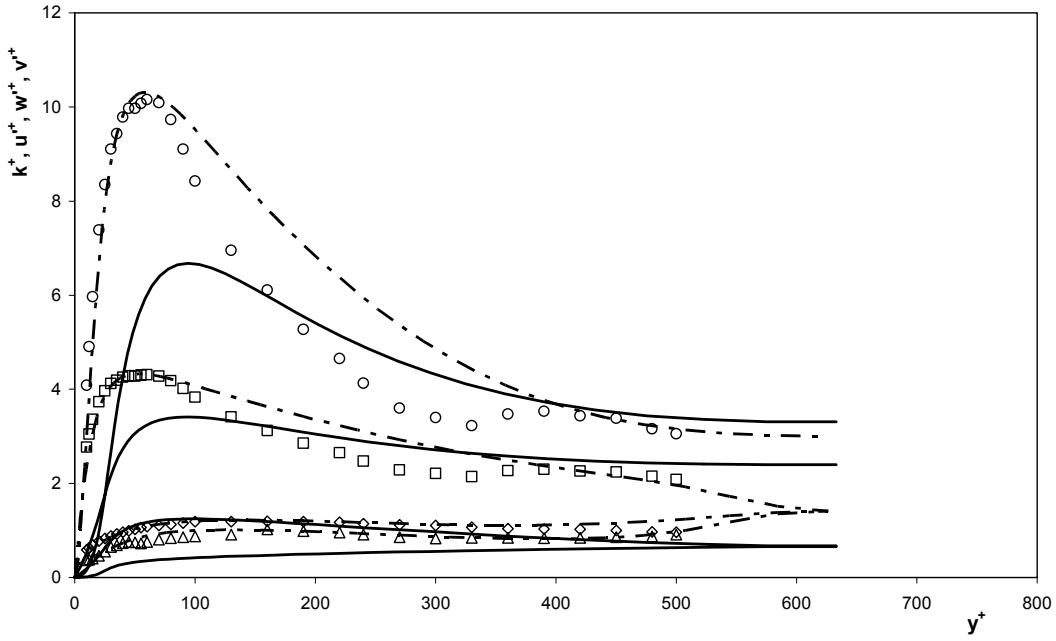

Fig. 5 – Comparison between the predicted and the measured profiles of normalized turbulent kinetic energy and Reynolds normal stresses for fully-developed turbulent pipe flow of 0.125% PAA fluid at Re=42900 in wall coordinates: ○ k^+ data of Escudier et al. [14];□ u'^+, ◊ w'^+, Δ v'^+ data of Resende et al. [6]; — Present model; — - Resende et al. [6].

For the 0.25% CMC fluid the predictions of f at different Reynolds number, and of the mean velocity profile and turbulent quantities at Re=16600 are presented in Fig. 6, Fig. 7 and Fig. 8, respectively. The slope of the predicted *f-Re* curve is lower than that of the experiments by a small amount and the mean velocity profile shows also a good agreement with the experiments.

In terms of the turbulent quantities, these are well predicted in terms of magnitude, but the peak axial normal stress and k are shifted to higher values of y^+.

The predictions of the Darcy friction factor for the two polymer solutions based on xantham gum (the blend of 0.09% CMC with 0.09% XG and 0.2% XG fluids) match very well the experimental data as shown in Fig. 9 and Fig. 10. There is a 16% difference in the value of f at Re=52400 for the blend, which decreases at lower Reynolds numbers. The opposite variation is observed to occur with the 0.2% XG fluid: now there is a 9% difference in f between the predictions and the experiments at Re=15000, which decrease with increasing Reynolds numbers.

It must be emphasised at this stage that the predictions for these two fluids, and in particular for the 0.2% XG solution, are significantly better than was previously achieved by any of the first-order closures developed in the past for viscoelastic fluids [1, 2, 6], an important success of the current Reynolds stress model.

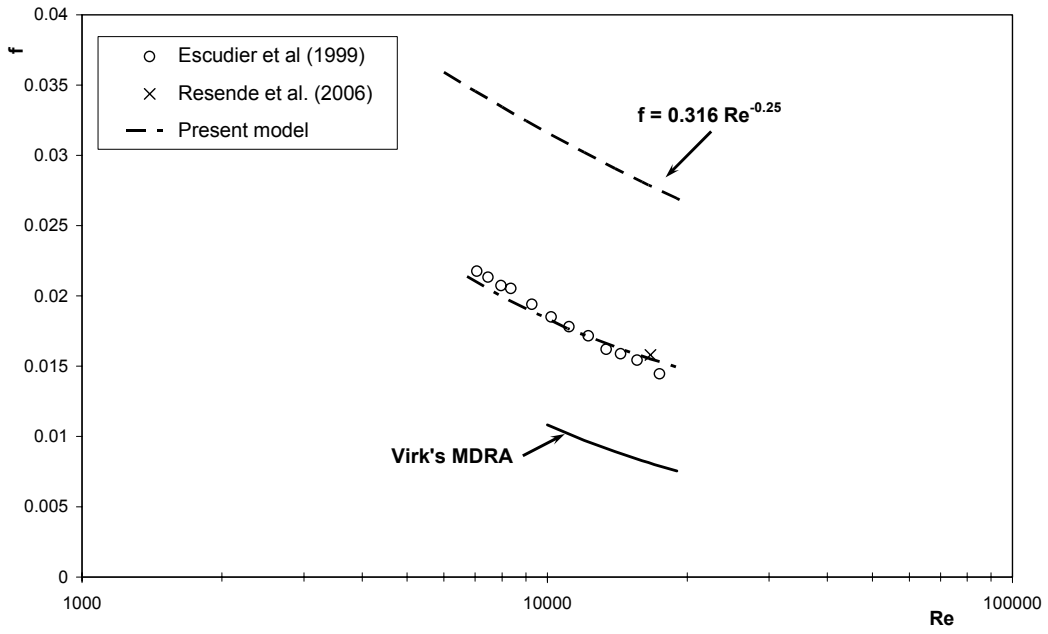

Fig. 6 – Comparison between predictions and measurements of Darcy friction factor in wall coordinates for fully-developed pipe turbulent flow with 0.25% CMC fluid.

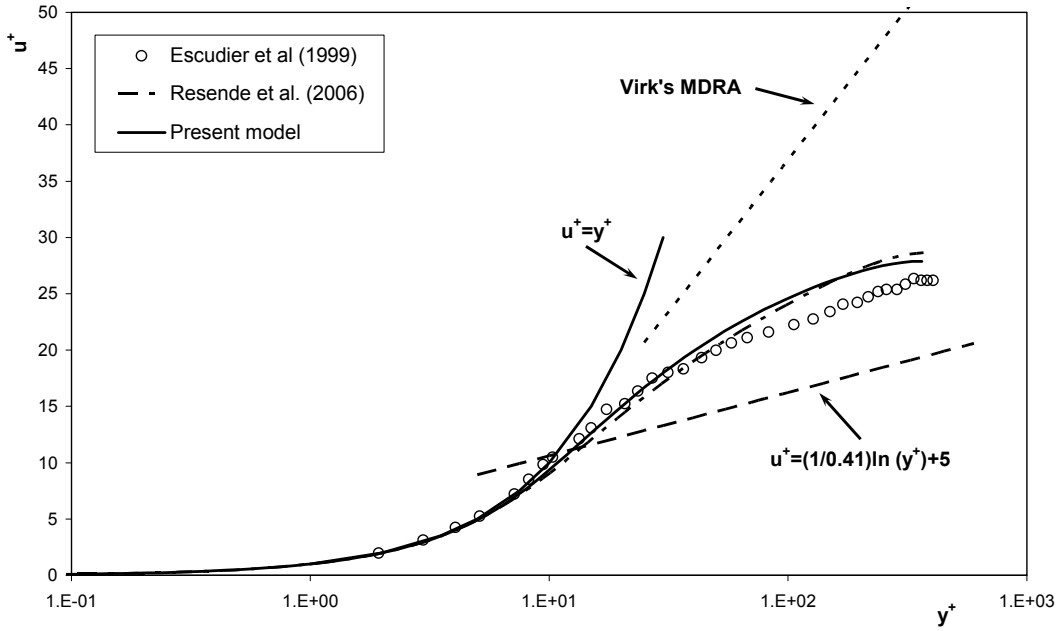

Fig. 7 – Comparison between the predicted and measured mean velocity profile for fully-developed pipe turbulent flow with the 0.25% CMC solution at Re=16600 in wall coordinates.

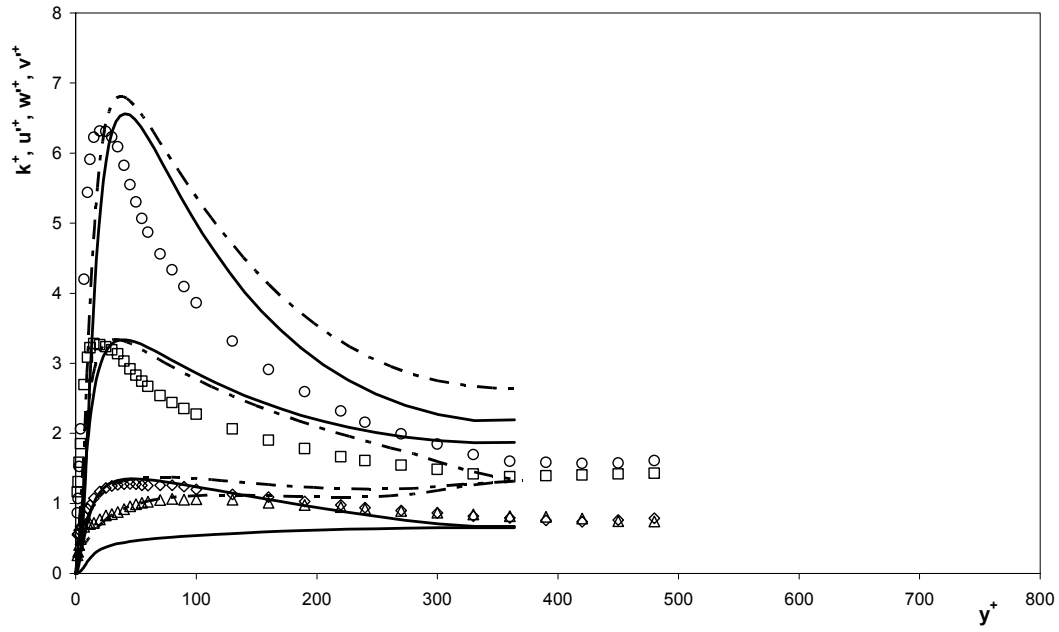

Fig. 8 – Comparison between the predicted and the measured profiles of normalized turbulent kinetic energy and Reynolds normal stresses for fully-developed turbulent pipe flow of 0.25% CMC fluid at Re=16600 in wall coordinates: ○ k^+ data of Escudier et al. [14];□ u'^+, ◊ w'^+, Δ v'^+ data of Resende et al. [6]; — Present model; — - Resende et al. [6].

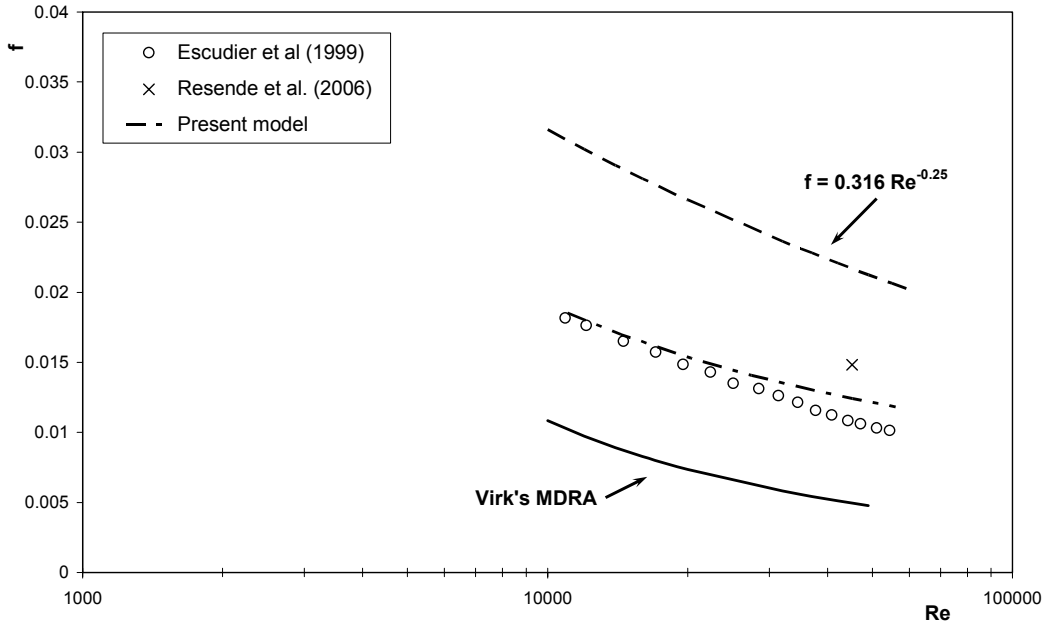

Fig. 9 – Comparison between predictions and measurements of Darcy friction factor in wall coordinates for fully-developed pipe turbulent flow with 0.09% / 0.09% CMC / XG fluid.

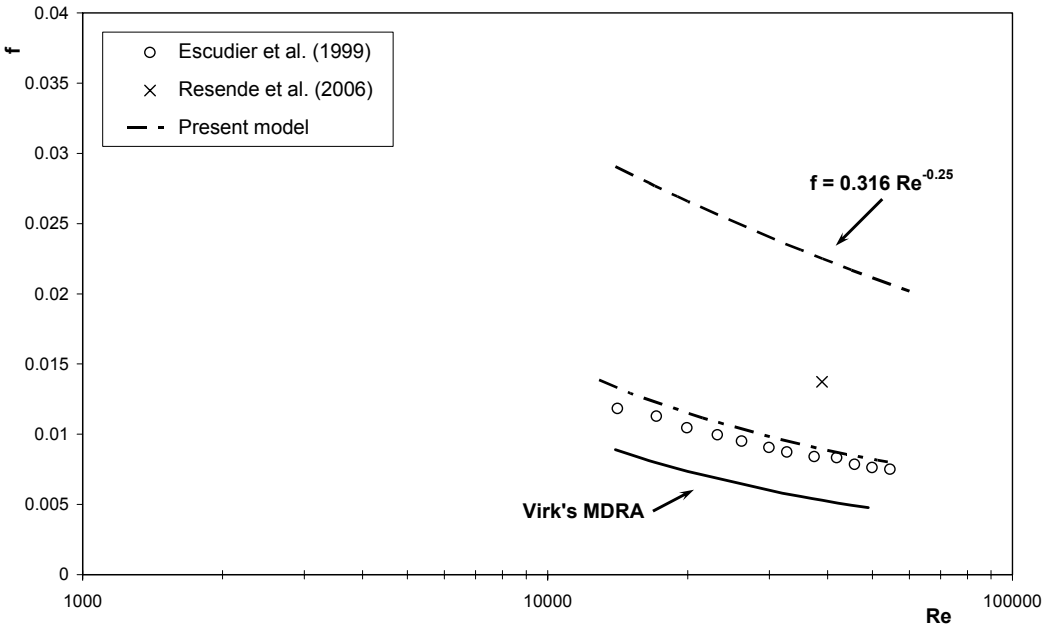

Fig. 10 – Comparison between predictions and measurements of Darcy friction factor in wall coordinates for fully-developed pipe turbulent flow with 0.2% XG fluid.

Similarly, predictions of the mean velocity profiles for the blend (0.09% / 0.09% CMC / XG) and the 0.2% XG solutions, at Re=45200 and Re=39000, respectively match the experimental

data, as seen in Fig. 11 and Fig. 12. Comparing with the previous model of Cruz et al. [2] there were significant improves, especially with the 0.2 XG fluids.
Fig. 13 for the blend and Fig. 14 for the 0.2% XG show that, as for the previous two non-Newtonian fluids, the axial and radial Reynolds normal stresses and *k* are underpredicted near the wall. For the 0.2% XG solution the tangential Reynolds normal stress is slightly over-predicted.
So, and as a general conclusion regarding predictions of the turbulent quantities, there is in almost all cases an underprediction in *k*, $\overline{u^2}$ and $\overline{v^2}$ near the wall, whereas $\overline{w^2}$ is usually well predicted.

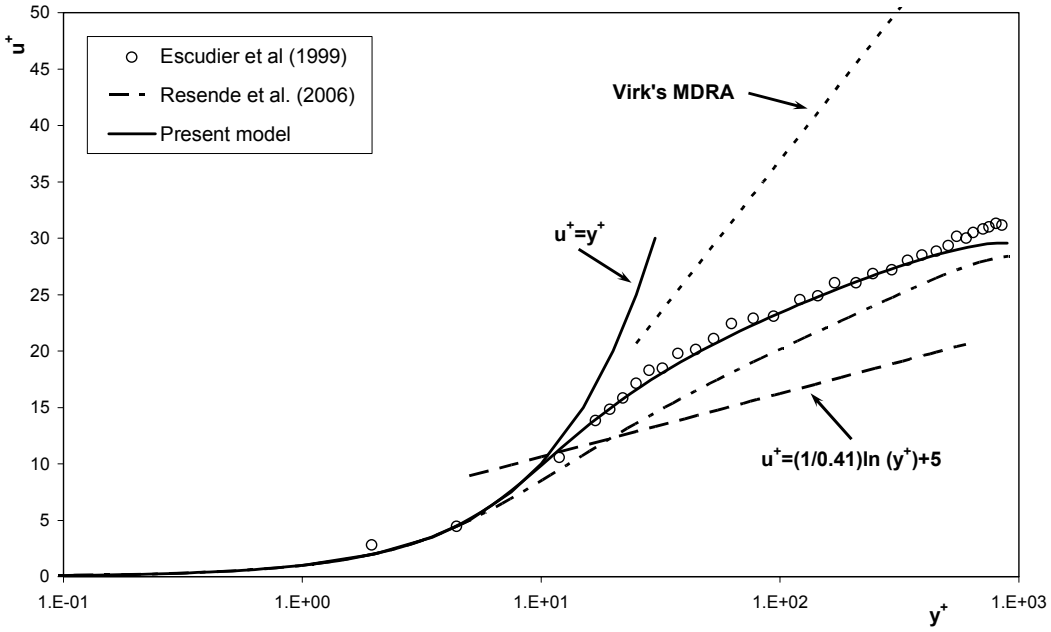

Fig. 11 – Comparison between the predicted and measured mean velocity profile for fully-developed pipe turbulent flow with the 0.09% / 0.09% CMC / XG solution at Re=45300 in wall coordinates.

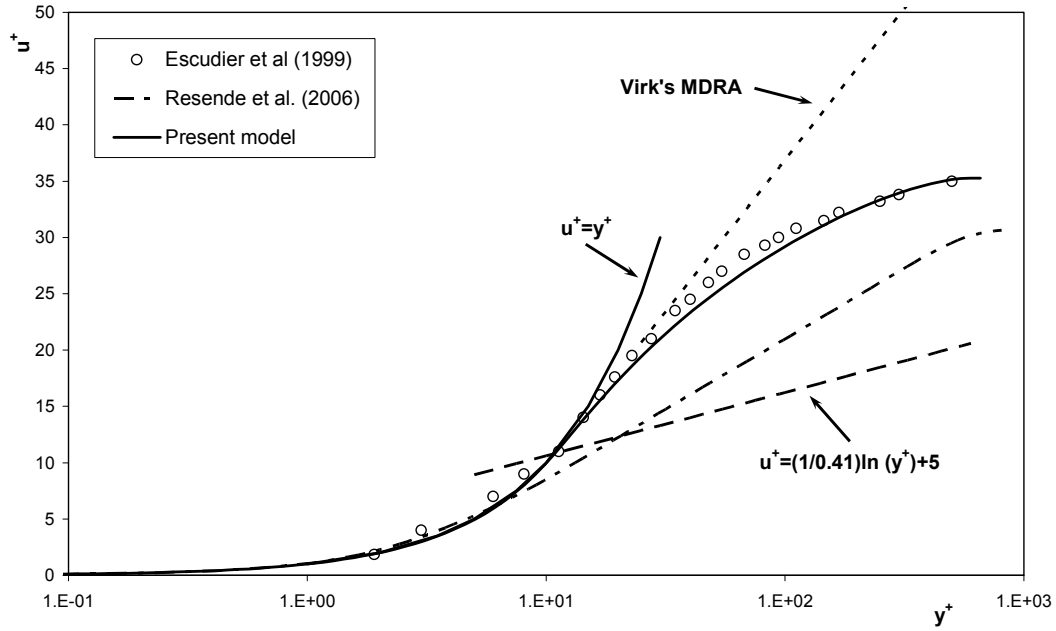

Fig. 12 – Comparison between the predicted and measured mean velocity profile for fully-developed pipe turbulent flow with the 0.2% XG solution at Re=3900 in wall coordinates.

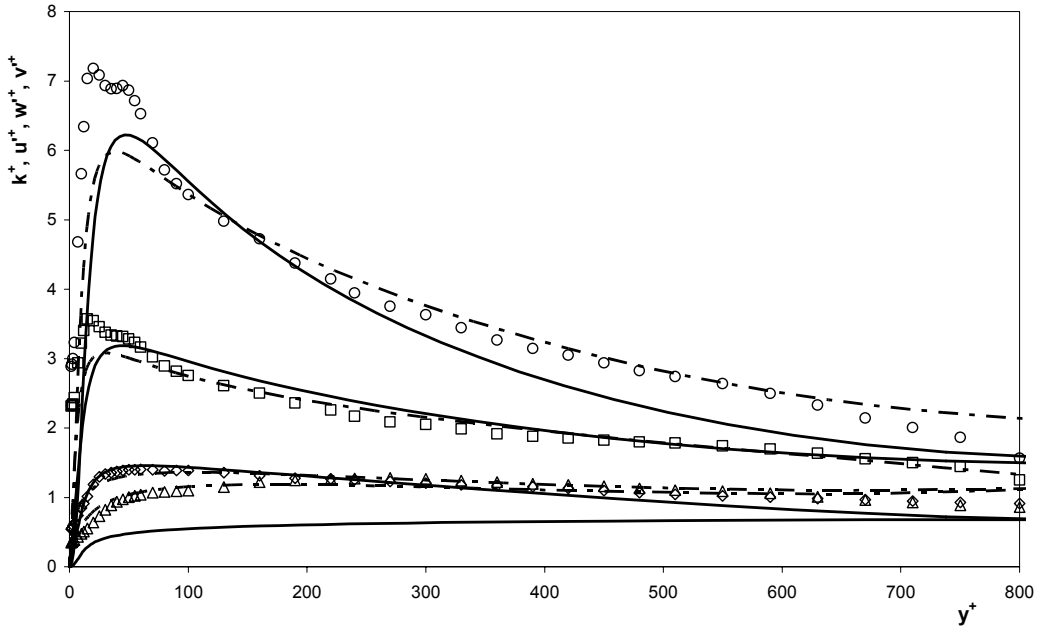

Fig. 13 – Comparison between the predicted and the measured profiles of normalized turbulent kinetic energy and Reynolds normal stresses for fully-developed turbulent pipe flow of 0.09% / 0.09% CMC / XG fluid at Re=45300 in wall coordinates: o k^+ data of Escudier et al. [14];□ u'^+, ◊ w'^+, Δ v'^+ data of Resende et al. [6]; — Present model; — - Resende et al.

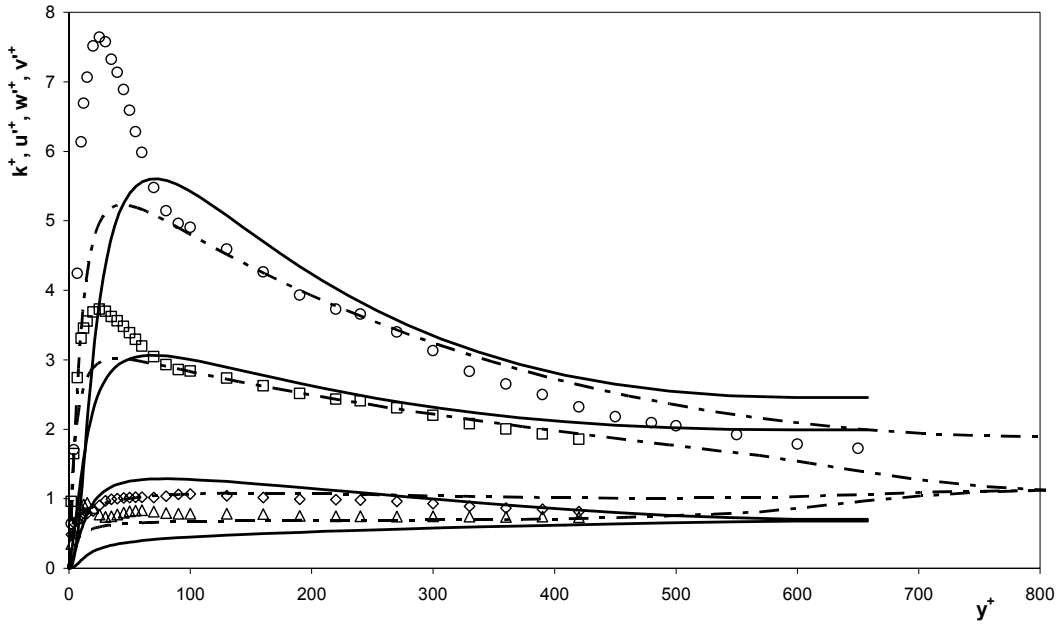

Fig. 14 – Comparison between the predicted and the measured profiles of normalized turbulent kinetic energy and Reynolds normal stresses for fully-developed turbulent pipe flow of 0.20% XG fluid at Re=39000 in wall coordinates: ○ k^+ data of Escudier et al. [14];□ u'^+, ◊ w'^+, Δ v'^+ data of Resende et al. [6]; — Present model; — - Resende et al.

4.2.2. DNS case

The present model was calibrated against experiments of 0.125% PAA and then tested against experiments with other polymer solutions. Here, we perform now a comparison of the predictions of this Reynolds stress model with the results from DNS calculations obtained by Dimitropoulos et al. [15] using a FENE-P model with L=10, β=0.9 and Re = 1994 (based on the bulk velocity and channel half-height). Our simulation was carried out using the following characteristics: half-height (H) of 50.2 mm; fluid density of 1000 kg/m^3; total zero shear viscosity of 0.01 Pa·s; η_{p0} = 0.001 Pa·s; η_s = 0.009 Pa·s; λ = 0.806 s. The shear and extensional viscosities of the FENE-P model and the fitted power law expressions used in the modified Generalized Newtonian model are plotted in Fig. 15 (a) and (b), respectively. Fig. 16 compares the predictions of the mean velocity profile with the DNS results and shows a good agreement. The predictions of turbulent kinetic energy in Fig. 17 are fair even though there is a deficit of the maximum value of k^+.

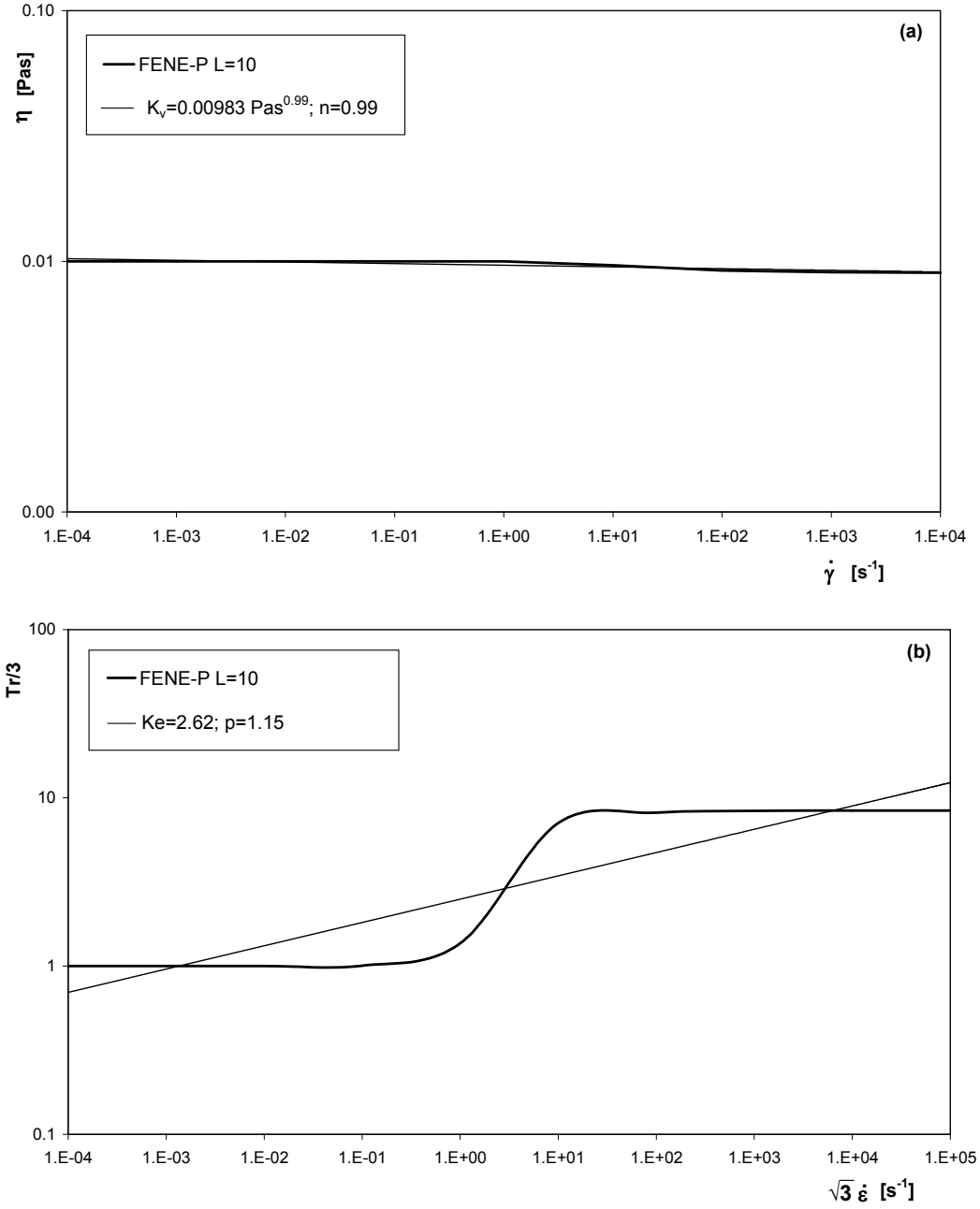

Fig. 15 – Comparison between the steady viscosities for the FENE-P model for L=10 and the modified GNF model: (a) shear viscosity; (b) extensional viscosity.

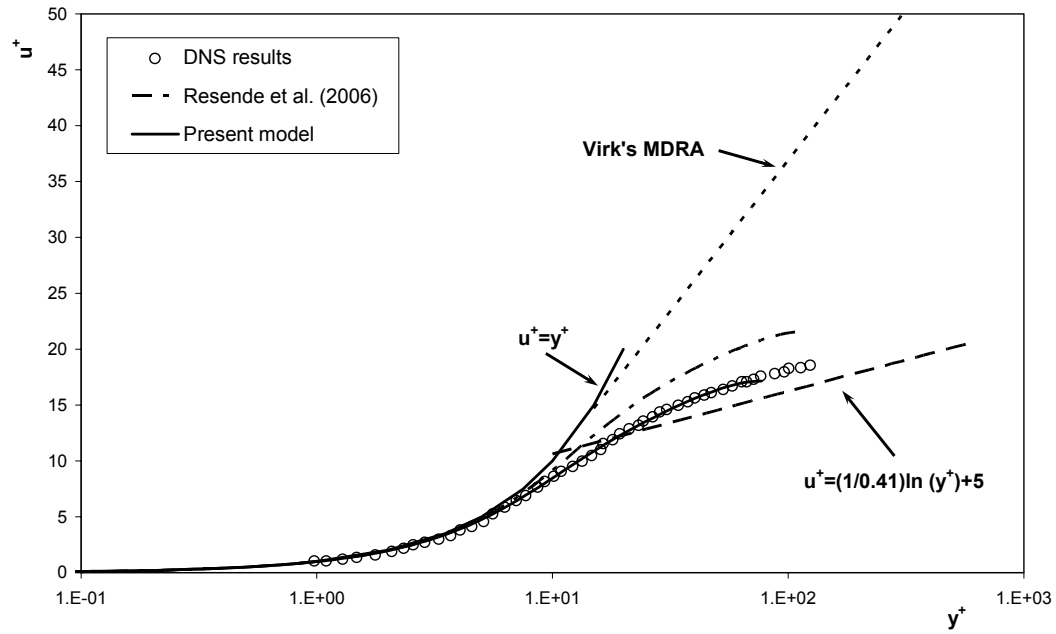

Fig. 16 – Comparison between the predictions and the DNS results of the mean velocity profile in wall coordinates for fully-developed pipe turbulent flow with FENE-P model, L=10, at Re=2100.

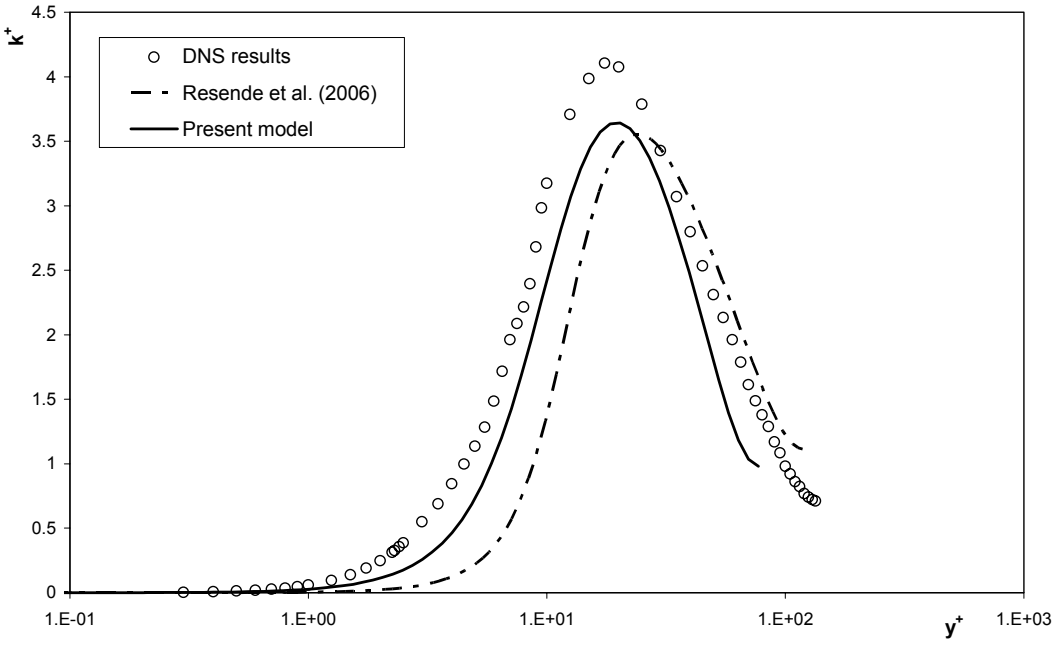

Fig. 17 – Comparison between the predictions and the DNS results of the turbulent kinetic energy profile in wall coordinates for fully-developed pipe turbulent flow with FENE-P model, L=10, at *Re*=2100.

5. CONCLUSIONS

A Reynolds stress model has been developed to predict the flow of viscoelastic solutions based on a generalised Newtonian constitutive equation modified to account for elastic effects. The Reynolds stress model is a modified version of the Lai and So [13] low Reynolds turbulence model which includes several new non-Newtonian terms. Closures for all these new terms were developed as well as for the pseudo-elastic stress term appearing in the momentum equation.

The predictions of this model are remarkably good for all fluids tested, four different aqueous solutions of polymer and this was assessed in terms of the friction factor, mean velocity and the three Reynolds normal stresses. The less successful achievement was in predicting these Reynolds stresses were in general the model underpredicted $\overline{u^2}$ near the wall, but it was able to predict well the $\overline{w^2}$ component.

A significant improvement over previous models for viscoelastic fluids are the successful predictions for the two solutions based on the semi-rigid xanthan gum molecule, for which the linear and nonlinear $k-\varepsilon$ models of Cruz et al. [2] and Resende et al. [6] underpredicted the measured levels of drag reduction.

Therefore, the present model represents a significant improvement over previous turbulence models for viscoelastic solutions, all of which are of first-order.

ACKNOWLEDGEMENTS

The authors would like to acknowledge funding of FEDER via projects POCI/56342/EQU/2004 and POCI/59338/EME/2004 of Fundação para a Ciência e Tecnologia.

BIBLIOGRAPHY

[1] D. O. A. Cruz and F. T. Pinho, *Turbulent pipe flow predictions with a low Reynolds number k-e model for drag reducing fluids*, Journal of Non-Newtonian Fluid Mechanics, Vol. 114, pp. 109-148, (2003).

[2] D. O. A. Cruz, F. T. Pinho and P. R. Resende, *Modeling the new stress for improved drag reduction predictions of viscoelastic pipe flow*, Journal of Non-Newtonian Fluid Mechanics, Vol. 121, pp. 127-141, (2004).

[3] V. C. Patel, W. Rodi and G. Scheuerer, *Turbulence Models for Near-Wall and Low Reynolds: A Review*, AIAA Journal, Vol. 23 (9), pp. 1308-1319, (1984).

[4] T. S. Park, H. J. Sung and K. Suzuki, *Development of a nonlinear near-wall turbulence model for turbulent flow and heat transfer*, Int. Journal of Heat and Fluid Flow, Vol. 24, pp. 29-40, (2003).

[5] T. J. Craft, B. E. Launder and K. Suga, *Development and application of a cubic eddy-viscosity model of turbulence*, Int. Journal of Heat and Fluid Flow, Vol. 17, pp. 108-115, (1996).

[6] P. R. Resende, M. P. Escudier, F. Presti, F. T. Pinho and D. O. A. Cruz, *Numerical predictions and measurements of Reynolds normal stresses in turbulent pipe flow of polymers*, Int. Journal of Heat and Fluid Flow, Vol. 27, pp. 204-219, (2006).

[7] T. Mizushina, H. Usui and T. Yoshida, *Turbulent pipe flow of dilute polymer solutions*, Journal Chem. Eng. Japan, Vol. 7 (3), pp. 162-167, (1973).

[8] F. Durst and A. K. Rastogi, *Calculations of turbulent boundary layer flows with drag reducing polymer additives*, Physics of Fluids, Vol. 20 (12), pp. 1975-1985, (1977).

[9] S. Hassid and M. Poreh, *A turbulent energy dissipation model for flows with drag reduction*, Journal of Fluids Engineering, Vol. 100, pp. 107-112, (1978).

[10] S. Politis 1989. *Turbulence modelling on inelastic power-law fluids*. Relatório interno, Departament of Mechanical Engineering, Imperial College of Science, Tecnology and Medicine, London, UK.

[11] M. R. Malin, *Turbulent pipe flow of power-law fluids*, Int. Commun. Heat Mass Transfer, Vol. 24 (7), pp. 977-988, (1997).

[12] F. T. Pinho, *A GNF framework for turbulent flow models of drag reducing fluids and proposal for a k-e type closure*, Journal of Non-Newtonian Fluid Mechanics, Vol. 114, pp. 149-184, (2003).

[13] Y. G. Lai and R. M. C. So, *On near-wall turbulent flow modelling*, Journal of Fluid Mechanics, Vol. 221, pp. 641-673, (1990).

[14] M. P. Escudier, F. Presti and S. Smith, *Drag reduction in the turbulent pipe flow of polymers*, Journal of Non-Newtonian Fluid Mechanics, Vol. 81, pp. 197-213, (1999).

[15] C. D. Dimitropoulos, R. Sureshkumar and A. N. Beris, *Direct numeric simulation of viscoelastic turbulent channel flow exhibiting drag reduction: effect of variation of rheological parameters*, Journal of Non-Newtonian Fluid Mechanics, Vol. 79, pp. 433-468, (1998).

[16] F. Durst, J. Jovanovic and J. Sender, *LDA measurements in the near-wall region of turbulent pipe flow*, Journal of Fluid Mechanics, Vol. 295, pp. 305-335, (1995).